Synthesis and luminescence properties of $BaBPO_5$:Ln, Na^+ (Ln = Eu^{3+}, Tb^{3+}, Dy^{3+}) phosphor in ultraviolet – visible region

JIE ZHANG, BING HAN*, YUANYUAN LIU, ZHIMENG WANG
School of Material and Chemical Engineering, Zhengzhou University of Light Industry, Zhengzhou 450002, People's Republic of China

A series of phosphors $Ba_{(1-2x)}Ln_xNa_xBPO_5$ (Ln = Eu^{3+}, Tb^{3+}, Dy^{3+}) with different x value were synthesized by using a solid-state reaction technique at high-temperature, and their photoluminescence properties were investigated in details. The f-f transitions of Eu^{3+}, Tb^{3+} and Dy^{3+} ions in the host lattice were assigned and discussed. The excitation and emission spectra indicate that $BaBPO_5$:Eu^{3+}, $BaBPO_5$:Tb^{3+} and $BaBPO_5$:Dy^{3+} can be effectively excited by near-ultraviolet, and exhibit reddish orange, yellowish green, and white light emission, respectively. The influence of the doping concentration on the relative emission intensity of Eu^{3+}/Tb^{3+}/Dy^{3+} in $BaBPO_5$ was also investigated. The present work suggests $BaBPO_5$: Ln, Na^+ (Ln = Eu^{3+}, Tb^{3+}, Dy^{3+}) phosphor can be a potential candidate as an UV-convertible phosphor for white light-emitting diodes (LEDs).

(Received December 02, 2013; accepted November 13, 2014)

Keywords: Phosphor, Luminescence, LEDs, $BaBPO_5$

1. Introduction

In recent years, more and more attention have been paid to the phosphor-converted white light emitting diodes (w-LEDs) [1-3], which can be classified into GaN chip with blue light emitting (440–470 nm) and InGaN chip with near ultraviolet (UV) emitting (350–420 nm) combined with phosphors. The commercial YAG:Ce^{3+} phosphor with yellow light emitting has been applied in the GaN chip, which possess low color-rendering index due to low color reproducibility on mass manufacturing scale and lack of red contents, respectively [4]. Thus, the near UV LEDs are expected to have greatly more potential application for solid-state lighting [5]. However, it is unfortunate that the present phosphors applied in near-UV InGaN-based LEDs are still some classic phosphors used in fluorescent lighting, which are not suitable for the near-UV LED chips because of the unbefitting absorption in the near-UV region [6, 7]. So it is essential to carry out relevant work to develop novel tricolor phosphors for near-UV LEDs.

Up to now, Eu^{3+}/Tb^{3+}/Dy^{3+} ions have been widely used as luminescence activator for phosphors and shows main red/green/white emissive components for fluorescence materials [8-10]. Meanwhile, strong absorption bands with the wavelength region from 350 nm to 400 nm can also be found in the excitation spectra for Eu^{3+}/Tb^{3+}/Dy^{3+} doped materials due to their 4f-4f transitions [11-13], which can match well with near-UV InGaN-based LEDs. So Eu^{3+}/Tb^{3+}/Dy^{3+} ions were chosen to be activators in this work.

$MBPO_5$[14, 15] (M = Ca, Sr, Ba) belongs to the stillwellite type compounds with the trigonal system, space group $P3_121$, M^{2+} ions are 10-fold coordinated by O^{2-} ions in the form of C_2 symmetry. The arrangements of BO_4^{5-} and PO_4^{3-} were loop-branched chains. The central three single chains of BO_4 tetrahedra run parallel to [0 0 1], the BO_4 units were linked to terminal PO_4 tetrahedra. Considering the excellent chemical and thermal stability of such kind of borophosphates, $BaBPO_5$ was chosen to be the host lattice in this work. So the main objective of this work is to investigate the preparation and spectroscopic properties of $BaBPO_5$:Ln^{3+}(Ln = Eu, Tb, Dy) phosphors in details in order to explore their potential application in w-LEDs.

2. Experimental

The phosphors $Ba_{(1-2x)}Ln_xNa_xBPO_5$ (Ln = Eu^{3+}, Tb^{3+}, Dy^{3+}) with different x value were synthesized by a high-temperature solid-state reaction technique. The starting materials are analytical reagent (A.R.) grade $BaCO_3$, H_3BO_3, $NH_4H_2PO_4$, Eu_2O_3 (99.99 %), Tb_4O_7 (99.99 %) and Dy_2O_3 (99.9 %). Na_2CO_3 (A.R.) was added as a charge compensator because the substitution of a Eu^{3+}/Tb^{3+}/Dy^{3+} ion for an alkaline earth ion requires the presence of a charge compensator to maintain overall

charge neutrality of the crystal. The chemical reaction equations are as follows:

$$2(1\text{-}2x)BaCO_3 + 2H_3BO_3 + 2NH_4H_2PO_4 + xLn_2O_3 + xNa_2CO_3 \rightarrow 2Sr_{(1-2x)}Eu_xNa_xBPO_5 + (2\text{-}3x)CO_2 + 2NH_3 + 5H_2O \ (Ln = Eu, Dy) \quad (1)$$

$$4(1\text{-}2x)BaCO_3 + 4H_3BO_3 + 4NH_4H_2PO_4 + xTb_4O_7 + 2xNa_2CO_3 + (2+x)CO \rightarrow 4Sr_{(1-2x)}Tb_xNa_xBPO_5 + (6\text{-}5x)CO_2 + 4NH_3 + 10H_2O \quad (2)$$

The stoichiometric reactants were mixed and ground thoroughly in an agate mortar. Finally the mixture was fired at 900 °C for 4 hours in air atmosphere for Eu^{3+}/Dy^{3+} doped samples and in CO atmosphere for Tb^{3+} doped samples. After the reaction at 900 °C, the products were cooled down slowly to room temperature (RT) by switching off the muffle furnace and ground into white power.

The phase purity and structure of the final products was characterized by a powder X-ray diffraction (XRD) analysis with Cu K_α (λ = 1.5405 Å) radiation on a D8 Advance X-Ray Diffractometer at 40 kV and 20 mA. Photoluminescence (PL) and photoluminescence excitation (PLE) spectra were measured on a fluorescence spectrometer (HITACHI F-7000) equipped with a 150 W xenon lamp as the excitation source at room temperature. The excitation and emission slits were set at 1 nm, all the spectra were measured at a scan speed of 240 nm/min.

3. Results and discussion

The XRD pattern of a $BaBPO_5$ sample is displayed in Fig. 1(a). It agrees with the JCPDS standard card and no impurity peaks are detected in the experimental range, which indicates the formation of a pure single $BaBPO_5$ phase. The samples Eu^{3+}/Tb^{3+}/Dy^{3+} doped $BaBPO_5$ with different doping concentration are also single phases that are in line with the undoped sample $BaBPO_5$ in Fig. 1(a) as well as the JCPDS 19-0096 [$BaBPO_5$] standard card. As examples, the diffractogram of samples $Ba_{0.92}Eu_{0.04}Na_{0.04}BPO_5$, $Ba_{0.84}Tb_{0.08}Na_{0.08}BPO_5$ and $Ba_{0.96}Dy_{0.02}Na_{0.02}BPO_5$ are exhibited in Figs. 1(b), 1(c) and 1(d), respectively. The above results show that a single phase was formed for the samples Eu^{3+}/Tb^{3+}/Dy^{3+} doped $BaBPO_5$ with different doping concentration, and the crystal structure of $BaBPO_5$ is not changed when the doped Eu^{3+}/Tb^{3+}/Dy^{3+} ions enter into the host lattice because of the similar ionic radius for Ba^{2+} and Eu^{3+}/Tb^{3+}/Dy^{3+} ions [16].

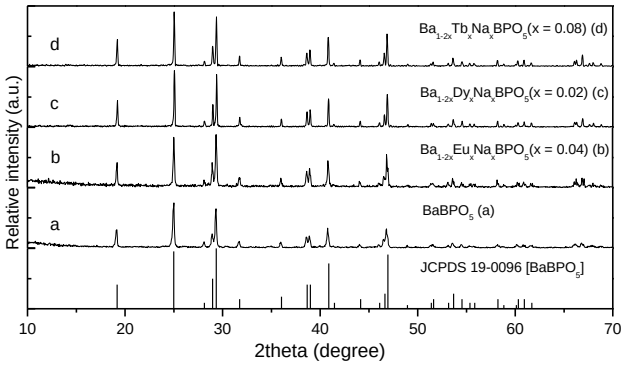

Fig. 1. The diffractogram of samples $BaBPO_5$ (a), $Ba_{0.92}Eu_{0.04}Na_{0.04}BPO_5$ (b), $Ba_{0.96}Dy_{0.02}Na_{0.02}BPO_5$ (c) and $Ba_{0.84}Tb_{0.08}Na_{0.08}BPO_5$ (d).

The excitation spectrum obtained by monitoring the $^5D_0 \rightarrow {}^7F_1$ transition of Eu^{3+} at 593 nm for the phosphor $Ba_{0.92}Eu_{0.04}Na_{0.04}BPO_5$ is shown in Fig. 2(a). A series of absorption lines from 280 nm to 500 nm can be observed in the curve a, which corresponds with the intra-configurational $4f^6$-$4f^6$ transitions of Eu^{3+} in $BaBPO_5$ host lattice. The narrow peaks correspond to the $^7F_0 \rightarrow {}^5F_J$ (298 nm), $^7F_0 \rightarrow {}^5H_6$ (318 nm), $^7F_0 \rightarrow {}^5D_4$ (361 nm), $^7F_0 \rightarrow {}^5G_2$(375/381 nm), $^7F_0 \rightarrow {}^5L_6$ (394 nm), $^7F_0 \rightarrow {}^5D_3$ (414 nm) and $^7F_0 \rightarrow {}^5D_2$ (464 nm) transitions of Eu^{3+}, respectively. Meanwhile, a broad band (marked as A) peaking at 264 nm between 220 nm and 280 nm is observed in curve a of Fig. 2(a), which is mainly related to the charge transfer (CT) transitions from completely filled 2p orbital of O^{2-} ion and the partially filled 4f orbital of the Eu^{3+} ion in the host lattice, since the location of the $O^{2-} \rightarrow Eu^{3+}$ CT band is in the range 200 ~ 300 nm in most borates and phosphates [17, 18]. It is found that the intensity of intra-configurational $4f^6$-$4f^6$ transitions was significantly stronger than that of CT transitions for Eu^{3+} ion, which is uncommon because the excitations of 4f–4f transitions for Eu^{3+} ion are parity forbidden in term of the selection rules, resulting in weak intensity. Some similar ones can be observed in other phosphors which show intense f–f absorption dominating the excitation process [19-21]. An effective charge can lead to this phenomenon, which has been discussed by Blasse and Van der Voort [22,23]. In our case, Eu^{3+} instituted Ba^{2+} sites in the $BaBPO_5$ host, and results in the positive effective charge, which induced a considerable nonradiative loss in the excited CT state of the Eu^{3+} ion. So, the 4f–4f transitions show more intense intensity than that of the CT band for Eu^{3+} ion.

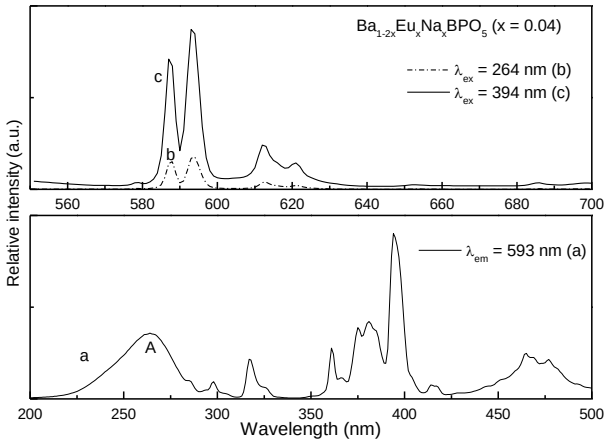

Fig. 2. The excitation (a) and emission (b, c) spectra of $Ba_{0.92}Eu_{0.04}Na_{0.04}BPO_5$.

The emission spectra of $Ba_{0.92}Eu_{0.04}Na_{0.04}BPO_5$ phosphor upon excitation at 264 nm and 394 nm are depicted in Figs. 2(b) and 2(c), respectively. The emission spectra are similar with each other, and are obviously composed of two groups of emission peaks, which are ascribed to the $^5D_0 \rightarrow {}^7F_1$ (587 nm, 593 nm) and $^5D_0 \rightarrow {}^7F_2$ (612 nm, 621 nm) transitions of Eu^{3+}, respectively. The strongest peaks located at 587 and 593 nm are attributed to the $^5D_0 \rightarrow {}^7F_1$ transition and the other peaks are weakened. Generally, it is thought that the $^5D_0 \rightarrow {}^7F_J$ emissions can give information on the site symmetry of Eu^{3+} in a specific host lattice. When the Eu^{3+} ion is located at crystallographic site with inversion symmetry, its magnetic-dipole transition $^5D_0 \rightarrow {}^7F_1$ orange emission dominates in the emission spectrum, while the electric-dipole transitions $^5D_0 \rightarrow {}^7F_2$ red emission is dominant if the Eu^{3+} site possesses an non-inversioncenter [8]. The above result indicated that the local symmetry of Eu^{3+} belongs to the inversion symmetry in the host lattice.

Fig. 3(a) shows the UV excitation spectrum of the sample $Ba_{0.84}Tb_{0.08}Na_{0.08}BPO_5$ at RT by monitoring the $^5D_4 \rightarrow {}^7F_5$ transition at 543 nm. The absorption peaks including the peaks of 305 nm ($^7F_6 \rightarrow {}^3H_6$), 320 nm ($^7F_6 \rightarrow {}^5D_0$), 343 nm ($^7F_6 \rightarrow {}^5L_7$), 353 nm ($^7F_6 \rightarrow {}^5L_9$), 371 nm ($^7F_6 \rightarrow {}^5G_5$), 379 nm ($^7F_6 \rightarrow {}^5G_6$) in the range of 300 ~ 400 nm (curve a) correspond to the f–f transitions of Tb^{3+} ions in the host lattice. The broad band A and B peaking at about 228 nm and 267 nm is ascribed to the spin-allowed and spin-forbidden f–d transition of Tb^{3+} ions, respectively. The reasons are as follows. For Tb^{3+} ions with $4f^8$ electron configuration, the ground states are ^7F_J. When one electron is excited into the 5d orbit, it gives rise to two $4f^75d^1$ excited states: a high-spin state with ^9D_J configurations with lower energy and a low-spin state with ^7D_J configurations with higher energy according to Hund's rule [24]. Therefore, Tb^{3+} in a specific host exhibits two groups of f–d transitions: the spin-allowed f–d transitions with high energy and the spin-forbidden f–d transitions with low energy. Therefore, the band B with peak maximum 267 nm is assigned to the lowest spin-forbidden f–d transitions of the Tb^{3+} ion, and the band A with peak maxima 226 nm is attributed to the spin-allowed f–d transitions of Tb^{3+}. So, the energy difference between the lowest spin-allowed f–d transition band (226 nm, 44248 cm^{-1}) and the lowest spin-forbidden f–d transition band (267 nm, 37453 cm^{-1}) is calculated to be 6895 cm^{-1}, which is close to the average value (6300 ± 900 cm^{-1}) for 19 compounds collected by Dorenbos [25, 26].

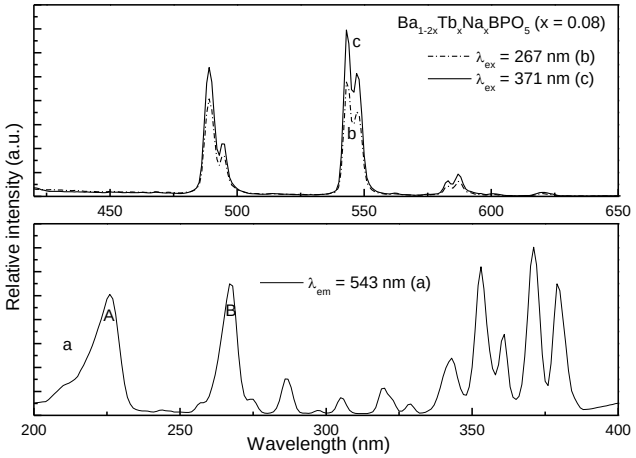

Fig. 3. The excitation (a) and emission (b, c) spectra of $Ba_{0.84}Tb_{0.08}Na_{0.08}BPO_5$.

The emission spectra of $Ba_{0.84}Tb_{0.08}Na_{0.08}BPO_5$ phosphor are depicted in Figs. 3(b) and 3(c). The emission spectrum under 266/371 nm excitation is composed of four emission peaks located at 489, 543, 587, and 618 nm, which are ascribed to the $^5D_4 \rightarrow {}^7F_6$, $^5D_4 \rightarrow {}^7F_5$, $^5D_4 \rightarrow {}^7F_4$ (weak) and $^5D_4 \rightarrow {}^7F_3$ (weak) transitions of Tb^{3+}, respectively, and the green $^5D_4 \rightarrow {}^7F_5$ emission at 543 nm is dominant. The emission of Tb^{3+} from $^5D_3$ level ($\lambda < 470$ nm) can not be observed clearly, suggesting the cross-relaxation ($^5D_3, {}^7F_6 \rightarrow {}^5D_4, {}^7F_0$) of Tb^{3+} occurring in this concentration.

The UV excitation spectra and the emission spectra under 348 nm excitation for the phosphor $Ba_{0.96}Dy_{0.02}Na_{0.02}BPO_5$ (x = 0.02) are shown in Fig. 4. Curve a displays the UV excitation spectrum by monitoring the emission of Dy^{3+} at 481 nm. A series of absorption lines can be observed in the curve a, which correspond with the intraconfigurational $4f^9$-$4f^9$ transitions of Dy^{3+} in $BaBPO_5$. The ground state of Dy^{3+} is $^6H_{15/2}$, the transition from this state to different excitation levels are read to be 295 ($^4K_{13/2}$, $^4H_{13/2}$, $^4F_{3/2}$, $^4D_{7/2}$), 323 ($^6P_{3/2}$), 348 ($^4I_{11/2}$, $^4M_{15/2}$, $^6P_{7/2}$), 363 ($^4P_{3/2}$, $^6P_{3/2}$, $^6P_{5/2}$), 385 ($^4M_{21/2}$, $^4I_{13/2}$, $^4F_{7/2}$) nm, respectively, in Fig. 4. The Dy^{3+}-O^{2-} charge-transfer band and $4f^9$-$4f^8$5d excitation band of Dy^{3+} were not observed in the short wavelength range. This is because they have popularly high energy, and located below 200 nm [10].

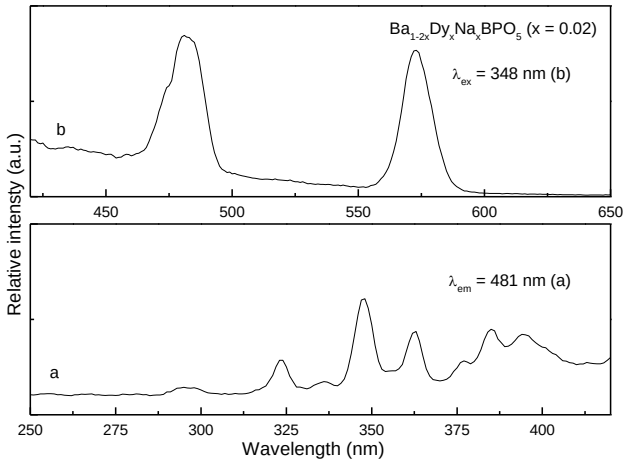

Fig. 4. The excitation (a) and emission (b) spectra of $Ba_{0.96}Dy_{0.02}Na_{0.02}BPO_5$.

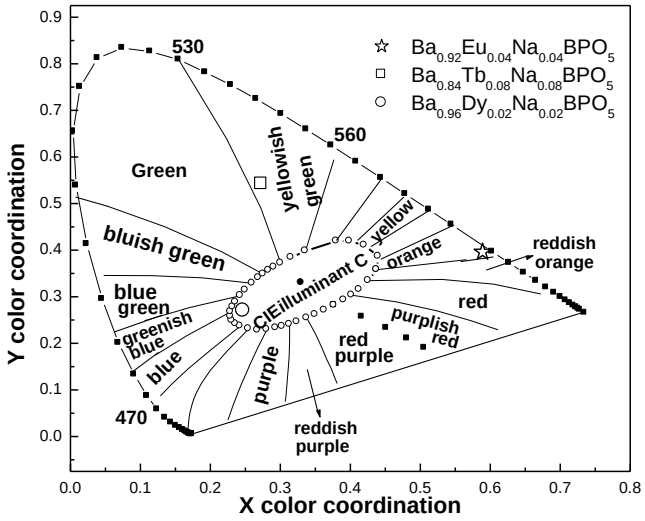

Fig. 5. The CIE chromaticity coordinates of the samples $Ba_{0.92}Eu_{0.04}Na_{0.04}BPO_5$, $Ba_{0.84}Tb_{0.08}Na_{0.08}BPO_5$ and $Ba_{0.96}Dy_{0.02}Na_{0.02}BPO_5$.

The emission spectra upon 348 nm excitation are exhibited in Fig. 4(b). Two $^4F_{9/2}\rightarrow{}^6H_J$ (J = 13/2, 15/2) lines are observed in the curve, in which the blue $^4F_{9/2}\rightarrow{}^6H_{15/2}$ emission at about 482 nm are strong, and whereas the yellow $^4F_{9/2}\rightarrow{}^6H_{13/2}$ emission at about 572 nm are weak. The crystal splitting components of Dy^{3+} emission can not be observed due to the weak experimental resolution. The $^4F_{9/2}\rightarrow{}^6H_{13/2}$ transition belongs to the hypersensitive transition with $\Delta J = 2$, which is strongly influenced by the local environment of Dy^{3+} in the host. So the Dy^{3+} site must be highly symmetric because the emission intensity of $^4F_{9/2}\rightarrow{}^6H_{15/2}$ transition is more than that of $^4F_{9/2}\rightarrow{}^6H_{13/2}$ transition. The result is similar with that in the Eu^{3+} in $BaBPO_5$.

Further, the CIE chromaticity coordinates of the samples $Ba_{0.92}Eu_{0.04}Na_{0.04}BPO_5$, $Ba_{0.84}Tb_{0.08}Na_{0.08}BPO_5$ and $Ba_{0.96}Dy_{0.02}Na_{0.02}BPO_5$ have been calculated from the PL spectra under the excitation of 394 nm, 371 nm and 348 nm, respectively. The chromaticity coordinates (x, y) are (0.596, 0.396), (0.262, 0.587) and (0.247, 0.270) for Eu^{3+}, Tb^{3+} and Dy^{3+} doped phosphor, which are shown in Fig. 5. The characteristic index shows that the Eu^{3+}, Tb^{3+} and Dy^{3+} doped phosphor has a deep reddish orange emission, yellowish green emission and white emission, respectively.

The luminescence intensity of phosphor materials is known to be dependent on the doping concentration of luminescent ions. The variation of emission intensity ($^5D_0\rightarrow{}^7F_1$ transition of Eu^{3+} at 593 nm, $^5D_4\rightarrow{}^7F_5$ of Tb^{3+} at 543 nm and $^4F_{9/2}\rightarrow{}^6H_{15/2}$) as functions of Eu^{3+}/Tb^{3+}/Dy^{3+} concentration under 393 nm/370 nm/348nm excitation is shown in Fig. 6, respectively. The most efficient luminescence intensities occur for a Eu^{3+} content of x = 0.04 and a Dy^{3+} content of x = 0.02. We do not observe the concentration quenching phenomenon in Tb^{3+} doped samples, which can be caused by the energy mismatch between $^5D_4\rightarrow{}^7F_6$ and $^5D_4\rightarrow{}^7D_J$ [27-29].

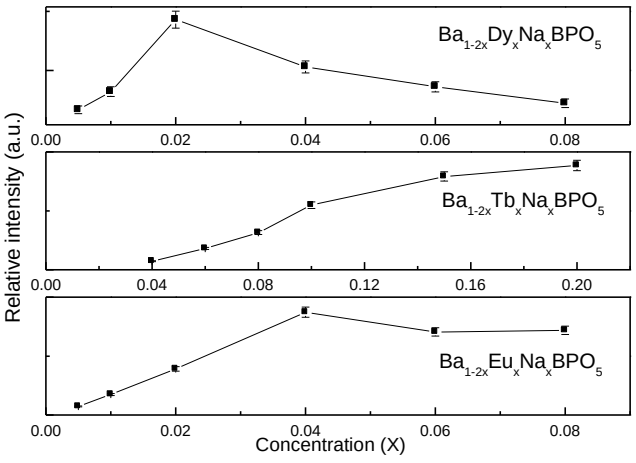

Fig. 6. The concentration dependence of the luminescence intensity of $Ba_{1-2x}Ln_xNa_xBPO_5$ (Ln = Eu, Tb, Dy) phosphors.

Luminescence characteristics including excitation wavelength, emission wavelength, chromaticity coordinates, optimal concentration, and emitting color are

shown in Table 1. As the excitation wavelength of $Ba_{1-2x}Ln_xNa_xBPO_5$ (Ln = Eu^{3+}, Tb^{3+}, Dy^{3+}) locates in the region from 340 nm – 400 nm, and matches well with the near-UV InGaN-based LED chips, so that these phosphors may be potential candidates as reddish orange, yellowish green, white phosphors for application in w-LEDs.

Table 1. Luminescence characteristics of $BaBPO_5:Ln^{3+}$ (Ln = Eu, Tb, Dy).

$Ba_{1-2x}Ln_xNa_xBPO_5$	Excitation wavelength (nm)	Emission wavelength (nm)	chromaticity coordinates (x, y)	Optimal concentration (x)	Emitting color
Ln = Eu	361, 375, 381, 394, 414	587, 593, 612, 621	0.596, 0.396	0.04	reddish orange
Ln = Tb	343, 353, 371, 379	489, 543, 587, 618	0.262, 0.587	−	yellowish green
Ln = Dy	343, 368, 385	482, 572	0.247, 0.270	0.02	white

4. Conclusions

In summary, $BaBPO_5$:Ln, Na^+ (Ln = Eu^{3+}, Tb^{3+}, Dy^{3+}) phosphors were prepared by a high-temperature solid-state reaction. The reddish orange emission of Eu^{3+}, yellowish green emission of Tb^{3+}, and white emission of Dy^{3+} are generated with CIE chromaticity coordinates of (0.596, 0.396), (0.262, 0.587), and (0.247, 0.270), respectively. The optimum doping concentration is 0.04 and 0.02 for Eu^{3+} and Dy^{3+} doped samples, respectively. The concentration quenching phenomenon was not observed in Tb^{3+} doped samples. It can be concluded that $BaBPO_5$:Ln, Na^+ (Ln = Eu^{3+}, Tb^{3+}, Dy^{3+}) phosphor is potentially a candidate as an UV-convertible phosphor for application in white LEDs.

Acknowledgments

The work is financially supported by the Science and Technology Project of Henan Province (no. 142300410245), the Science and Technology Research Key Project of Education Department of Henan Province (no. 12A430021), and the Scientific Research Fund of Zhengzhou University of Light Industry (2013XJJ003).

References

[1] R. J. Xie, N. Hirosaki, N. Kimura, et al., Appl. Phys. Lett. **90**, 191101 (2007).
[2] S. C. Allen, A. J. Steckl, Appl. Phys. Lett. **92**, 143309 (2008).
[3] K. H. Lee, S. H. Park, H. S. Yoon, et al., Opt. Express **20**, 6248 (2012).
[4] Y. Chen, J. Wang, X. G. Zhang, et al., Sens. Actuators B **148**, 259 (2010).
[5] E. Radkov, R. Bompiedi, A. M. Srivastava, et al., Proc. SPIE **5187**, 171 (2004).
[6] S. Neeraj, N. Kijima, A. K. Cheetham, Chem. Phys. Lett. **387**, 2 (2004).
[7] V. Sivakumar, U. V. Varaduaraju, Electrochem. Solid-State. Lett. **9**, 35 (2006).
[8] B. Han, H. B. Liang, H. Y. Ni, et al., Opt. Express **17**, 7138 (2009).
[9] B. Han, H. B. Liang, Y. Huang, et al., J. Phys. Chem. C **114**, 6770 (2010).
[10] B. Han, H. B. Liang, H. H. Lin, et al., J. Opt. Soc. Am. B **25**, 2057 (2008).
[11] D. Balaji, A. Durairajan, K. Kavi Rasu, et al., J. Lumin. **146**, 458 (2014).
[12] R. Sankar, Opt. Mater. 31, 268 (2008).
[13] I. M. Nagpure, V. B. Pawade, S. J. Dhoble, Lumin. **25**, 9 (2010).
[14] R. Kniep, G. Gozel, B. Eisenmann, et al., Angew. Chem. Int. Ed. Engl. **33**, 749 (1994).
[15] S. Pan, Y. Wu, P. Fu, et al., Chem. Mater. **15**, 2218 (2003).
[16] R. D. Shannon, Acta Crystallogr. A **32**, 751 (1976).
[17] P. Dorenbos, J. Lumin. **111**, 89 (2005).
[18] P. Dorenbos. J. Phys.: Condens. Matter **15**, 8417 (2003).
[19] M. M. Haque, M. A. Asraf, M. F. Hossen, et al., J. Alloys Comp. **539**, 195 (2012).
[20] Q. Liu, Y. Liu, Z. Yang, et al., Spectrochim. Acta, Part A **87**, 190 (2012).
[21] R. J. Yu, H. M. Noh, B. K. Moon, et al.. J. Alloys Comp. **576**, 236 (2013).
[22] D. Van der Voort, G. Blasse, J. Solid State Chem. **99**, 404 (1992).
[23] D. Van der Voort, G. Blasse, Chem. Mater. **3**, 1041 (1991).
[24] B. Han, H. B. Liang, H. H. Lin, et al.. Appl. Phys. A **88**, 705 (2007).
[25] P. Dorenbos, J. Lumin. **91**, 155 (2000).
[26] P. Dorenbos, J. Lumin. **91**, 91 (2000).
[27] Y. Y. Choi, K. S. Sohn, H. D. Park, et al., J. Mater. Res. **16**, 881 (2001).
[28] K. S. Sohn, Y. Y. Choi, H. D. Park, et al., J. Electrochem. Soc. **147**, 2375 (2000).
[29] K. S. Sohn, Y. G. Choi, Y. Y. Choi, et al., J. Electrochem. Soc. **147**, 3552 (2000).

*Corresponding author: hanbing@zzuli.edu.cn